Simulation of Fluorescence Anisotropy Experiments: Probing Protein Dynamics

Gunnar F. Schröder,* Ulrike Alexiev,[†] and Helmut Grubmüller*

*Theoretical and Computational Biophysics Department, Max-Planck-Institute for Biophysical Chemistry, Göttingen, Germany; and
[†]Department of Physics, Freie Universität Berlin, Berlin, Germany

ABSTRACT   Time-resolved fluorescence anisotropy decay experiments on a protein-attached dye can probe local protein dynamics and steric restrictions, but are difficult to interpret at the structural level. Aiming at an atomistic description, we have carried out molecular dynamics simulations of such experiments. Our simulations describe an Alexa488 fluorescent dye male-imide derivative covalently attached via a single cysteine to the AB-loop of bacteriorhodopsin. Fluorescence anisotropy decay curves obtained from the simulations agree well with the measured ones. Three anisotropy decay components were resolved and assigned to: 1), the fast dynamics of the attached dye on the picosecond timescale; 2), the slower dynamics of the loop at the one nanosecond timescale; and 3), the overall tumbling of the molecule. For the biologically relevant 1-ns component we identified two processes from simulations, the motion of the flexible loop as well as slow conformational dynamics of the dye. These two processes are not separable by experiment alone. Furthermore, analysis of the correlation between the dye and the protein motion revealed which part and which motion of the protein is actually probed by the experiment. Finally, our simulations allowed us to test the usual and inevitable assumption underlying these types of spectroscopic measurements that the attached dye probe does not severely perturb the protein dynamics. For the case at hand, by comparison with a simulation of the dye-free protein, the perturbation was quantified and found to be small.

INTRODUCTION

Protein motions, particularly their conformational dynamics, regulate and often constitute protein function. Therefore, a large variety of experimental and theoretical techniques aim at probing internal dynamics of proteins, with a particular focus at the picosecond to microsecond timescale. Nuclear magnetic resonance, electron paramagnetic resonance, neutron scattering, as well as fluorescence depolarization experiments have indeed provided much insights in this respect.

Fluorescence spectroscopy, in particular, in combination with site-directed fluorescent labeling has become an established tool to investigate the dynamics and interactions of biomolecules. Fluorescence resonance energy transfer experiments allow us to determine intramolecular distances in biomolecules (1,2), recently even with millisecond time resolution (3–5). Time-resolved fluorescence anisotropy experiments provide information on both, mobility and dynamics of a fluorophore (6,7). Because this probed dynamics of the dye is affected by the motion of the protein fragment to which it is attached, the anisotropy decay yields information on the protein structure and conformational changes as well as on the protein flexibility. Recently, this approach has been successfully applied to surface loop dynamics of rhodopsin and bacteriorhodopsin (bR), where an anisotropy decay component could be assigned to the loop motion, which allowed for the identification of protein conformational changes (8).

To extract structural information from the anisotropy decay curves is not straightforward, however. Several empir-ical models have therefore been proposed to facilitate the interpretation (9–12). Accordingly, many results obtained by these experiments depend on the particular choice of model used. Furthermore, each model rests on certain assumptions that are not always easy to verify. A first-principles simulation approach, in contrast, would enable one to drop these assumptions and thus to provide more accurate interpretations of the experiments at the molecular level. To this aim, we have carried out molecular dynamics (MD) simulations of the complete experimental system including the protein, the protein-attached dye and an explicit solvent environment. These simulations should allow us to extract the individual contributions to the depolarization and to analyze the dye-protein interactions at atomic detail.

In a similar spirit, but at faster timescales, MD simulations of tyrosine- and tryptophan-containing proteins have been used to predict the fluorescence anisotropy decay function (13–17). Furthermore, anisotropy decay measurements of a dye attached to flexible protein regions have been correlated with side-chain dynamics from MD simulations (18). Also, simulations of free fluorophores in a solvent reproduced temperature and solvent dependence of the experimental fluorescency anisotropy (19,20). In particular, the rotational diffusion of tryptophan in water has been simulated and its dependency on different water models discussed (21,22).

Here, and in contrast to the previous studies, the focus is on the interaction and dynamic coupling between a particular protein fragment and the attached dye. In addition, determination of dye conformation often is a key to the interpretation of fluorescence spectroscopy experiments. We will show that dye conformations can also be obtained from MD

simulations, which therefore provide valuable information complementary to the experiment.

The system studied here is a fragment of the heptahelical transmembrane protein bR, which shares the heptahelical bundle motif with the large class of G-protein coupled receptors (GPCRs) and is considered a prototype for GPCRs. In general, GPCRs participate within many cell signaling pathways by conversion of external stimuli into intracellular responses. The dynamics and flexibilities of surface-exposed protein loops of these GPCRs have been shown to play a crucial role in activation and molecular recognition of the receptor, as G-proteins transduce the conformational change of the activated receptor into a regulated effector function (for recent reviews, see Sakmar et al. (23) and Marshall (24)). Investigation of the local protein surface dynamics and flexibility can thus provide much insight into the mechanism of receptor activation and signal protein binding to the protein surface. Recent picosecond time-resolved fluorescence anisotropy decay measurements (8) have addressed the dynamics of these loops.

Here we report on a combined MD simulation and experimental approach, where both, measurements and simulations have been devised to match each other as closely as possible. In the experiments, and in the simulations we used the C_5 maleimide of the fluorescent dye Alexa488 covalently bound to a single cysteine residue introduced at position 35 of bR to probe the flexibility of the loop connecting the first two transmembrane helices A and B. In close analogy to the experimental design used for the assignment of the loop component (8), the AB fragment of bR has been studied at first to characterize the intrinsic dynamics of the AB loop. In a next step, comparison with loop dynamics of the intact protein is feasible and is expected to provide information on the interactions between the loops.

Our aim in this study is to gain insight into fluorescence anisotropy experiments by providing an interpretation of the experiment in atomic detail. We particularly address the following questions: Which processes influence the reorientational dynamics of the dye? What are the individual contributions to the observed depolarization? How does one extract information on the protein conformational dynamics from the anisotropy decay curve? Vice versa our simulations should enable us to study to what extent does the attached dye affect the unperturbed loop dynamics. This effect is commonly—and necessarily—assumed to be small. This study offers the chance to test this assumption.

THEORY: FLUORESCENCE ANISOTROPY

Here we summarize the basic equations that will be used to calculate anisotropy decay curves from molecular dynamics simulations as well as from experiments. In the experiments, dye molecules are excited by a short polarized laser pulse. After a period of time t, during which the dye has undergone rotational diffusion, the polarization of the reemitted light is measured. The fluorescence anisotropy $r(t)$ at time t after excitation of the fluorophore is defined as

$$r(t) = \frac{I_\parallel(t) - I_\perp(t)}{I_\parallel(t) + 2I_\perp(t)}, \tag{1}$$

where $I_\parallel(t)$ and $I_\perp(t)$ are the measured parallel and perpendicular fluorescence intensities, respectively, with respect to the field vector of the exciting light pulse. Assuming an ensemble of fluorophores with random isotropic initial orientations, $r(t)$ is given by

$$r(t) = \frac{2}{5}\langle P_2[\boldsymbol{\mu}_a(s) \cdot \boldsymbol{\mu}_e(s+t)]\rangle, \tag{2}$$

where $\boldsymbol{\mu}_a(t)$ and $\boldsymbol{\mu}_e(t)$ are normalized absorption and emission dipole moment vectors, respectively (9,25). $P_2(x) = (3x^2 - 1)/2$ is the second-order Legendre polynomial. Time $t = 0$ is defined as the time of excitation by the short polarized laser pulse in the experiment. Here, assuming a sufficiently ergodic MD trajectory, the ensemble average $\langle \rangle$ will be approximated by a time average. In the simplest case of isotropic rotational diffusion of a fluorophore, the anisotropy shows a monoexponential decay to zero with a decay or rotational correlation time ϕ, which is determined by the rotational diffusion coefficient. Note that absolute fluorescence intensities do not appear in Eq. 2, as they cancel out in Eq. 1. Therefore, the fluorescence lifetime has not to be considered in the simulations.

For the case at hand, where the dye has been attached to a protein, the motional freedom of the dye is restricted. A common model to describe such restricted rotational diffusion, which we will also use as a reference, is the "wobbling-in-a-cone" model (9). In this model, the transition dipole is assumed to diffuse freely inside a cone (Fig. 1, *top*) fixed within the molecular frame, and the anisotropy $r(t)$ can be approximated by

$$r(t) = r_0\left[(1 - A_\infty)e^{-t/\phi} + A_\infty\right]. \tag{3}$$

Here, $r_0 = 0.4\,P_2(\cos \lambda)$, and λ is the angle between the absorption and emission dipole moment fixed in the coordinate frame of the dye. A_∞ is a parameter describing the degree of motional restriction and is related to the semicone angle θ_{max} (Fig. 1 A) by

$$A_\infty = \frac{r_\infty}{r_0} = \left[\frac{1}{2}(1 + \cos \theta_{max})\cos \theta_{max}\right]^2. \tag{4}$$

Note that a small cone angle gives rise to a large value of A_∞; vice versa, A_∞ vanishes for isotropic rotational diffusion. Additionally considering an isotropic overall tumbling motion of the dye-protein complex as a whole, described by a rotational correlation time ϕ_G, the anisotropy of the protein-attached dye is given by

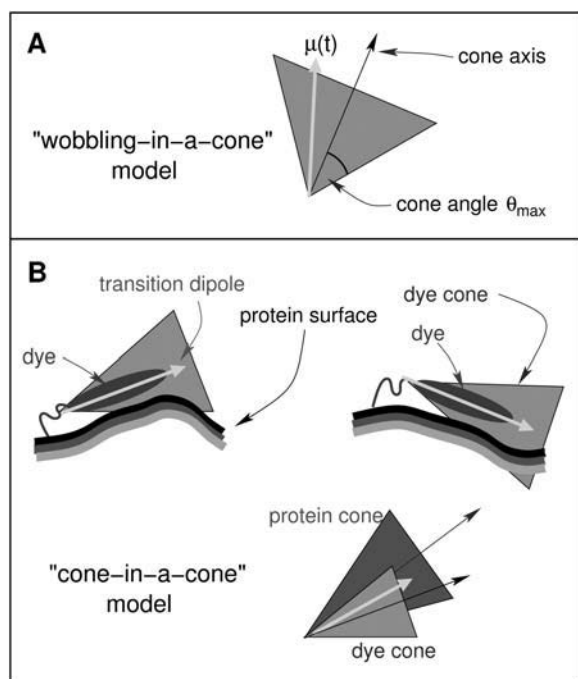$$r(t) = r_0[(1 - A_\infty)e^{-t/\phi} + A_\infty]e^{-t/\phi_G}. \tag{5}$$

FIGURE 1 (*A*) Wobbling-in-a-cone model. The transition dipole moment $\mu(t)$ is assumed to freely diffuse inside a cone with the semicone angle θ_{max}. (*B*) Cone-in-a-cone model. The two top figures indicate a motion, which is due to the protein flexibility, superimposed to the wobbling-in-a-cone model. The bottom figure visualizes how the protein flexibility is described in the cone-in-a-cone model by the protein cone, within which the dye cone freely diffuses.

The orientational dynamics of the dye is also affected by the local flexibility of the protein, which is of particular interest here. The resulting surface changes affect cone orientation and possibly, also cone angle (Fig. 1 *B*, *top*). In a simple model (14), also these protein-induced changes are described by a restricted motion of the dye cone within a (second) cone (Fig. 1 *B*, *bottom*). Assuming that the local dye motion and the protein dynamics are uncoupled, this effect gives rise to a second decay factor,

$$r(t) = r_0[(1 - A_1)e^{-t/\phi_1} + A_1][(1 - A_2)e^{-t/\phi_2} + A_2] \; e^{-t/\phi_G}. \tag{6}$$

It is therefore referred to here as the ''cone-in-a-cone'' model.

MATERIAL AND METHODS

Fluorescence anisotropy experiment

Sample preparation

The preparation and expression of the bR mutant S35C in *Halobacterium salinarium*, in which cysteine replaces Ser-35, has been reported (27). Solubilization of bR membrane fragments and regeneration of bR in DMPC/CHAPS-micelles were performed as reported (27). The regeneration procedure was modified according to protocols described (28). Briefly, bR membrane fragments were solubilized in 1.2% (w/v) SDS and 1 mM DTT. After

the retinal band is shifted completely to ~380 nm the excess SDS was removed by chromatography on Sephadex-G25, preequilibrated, and eluted with 0.1% SDS in 5 mM sodium phosphate buffer at pH 6. The regeneration was started by adding 2% CHAPS/2% DMPC, 20 mM sodium phosphate buffer, pH 6.2, and 400 mM KCl. After regeneration excess lipids, detergents and buffer were removed by chromatography on Sephadex-G25, preequilibrated, and eluted with 0.1% CHAPS and 150 mM KCl. The retinal band is shifted back completely to 550 nm, resulting in 96–100% regeneration, using an estimated extinction coefficient of $\epsilon_{550} \approx 52,000$ $M^{-1}cm^{-1}$. Labeling of bR with Alexa488 and the determination of the labeling stoichiometry were performed as described (29) for 5- (iodoacetamido)-fluorescein and adapted for Alexa488 C_5 maleimide (Molecular Probes, Eugene, OR). The reaction of 50 μM bR with 2 mM fluorescent label was carried out at room temperature in 150 mM KCl, 100 mM Tris buffer, pH 8.0, 30 mM EDTA, 200 μM DTT. Excess reagents were removed by chromatography on Sephadex G-25 in 0.1 A 10-mM stock solution of the respective label was used. The labeling stoichiometry was calculated using

$$c_{Label}/c_{bR} = (\Delta A_L/\epsilon_L)(\epsilon_{bR}/A_{550}), \tag{7}$$

where c_{Label} and c_{bR} are the molar concentrations of the bound fluorescent label and bR, respectively. ΔA_L is the absorbance difference at the λ_{max} of the label; ϵ_L is the molar extinction coefficient of the label (from Molecular Probes). A_{550} is the absorbance of the bR sample at 550 nm with $\epsilon_{bR} = 52,000$ M^{-1} cm^{-1}. The preparation of proteolytically cleaved fragments of bR with chymotrypsin were performed according to the method described (30). The digestion procedure was applied to the bR mutant S35C labeled with Alexa488. The incubation time was restricted to 30 min at 37°C. This results in incomplete digest, but prevents further cleavage of the fragment 1–72. The fragments containing residues 1–72 were separated by centrifugation with microcentrifuge filters Centrisart-C4 with 10,000 molecular weight cutoff. The fragments obtained showed a single fluorescent band by SDS-PAGE below 10 kDa for the fluorescently labeled fragment 1–72 and a further band at 26 kDa for the undigested bacteriorhodopsin (Fig. 2 *A*, lanes *2* and *3*). A secondary structural model of the AB-helix fragment is shown in Fig. 2 *B* and residue S35C is circled. The absorption and emission spectra of the Alexa488 labeled bacteriorhodopsin are shown in Fig. 3.

Time-resolved fluorescence depolarization experiments

The proteolytically cleaved fragments of the fluorescently labeled bR mutant S35C containing residues 1–72 were used as a model 2-helix system (Fig. 2 *B*) to analyze the anisotropic behavior of the fluorescent dye in its protein bound state (8). Before time-resolved fluorescence measurements, the AB-helix fragment was concentrated and dissolved in methanol.

The fluorescence anisotropy decays were measured employing a tunable Ti:sapphire laser/microchannel plate-based single-photon counting apparatus with picosecond time resolution. A detailed account of the experimental setup has already been provided (8). This method allows to measure the diffusional dynamics of the loops directly on the pico- to nanosecond timescale. The fluorescence decay profiles, $I_{\parallel}(t)$ and $I_{\perp}(t)$ or $I_{\parallel}(t) + 2I_{\perp}(t)$, and the time-resolved anisotropy as given by Eq. 1 were analyzed using the software package Global Unlimited V2.2 (Laboratory for Fluorescence Dynamics, University of Illinois, Urbana, IL). The time course of the fluorescence was deconvoluted and fitted with a sum of exponentials

$$I(t) = \sum_{i=1} \alpha_i \exp(-t/\tau_i). \tag{8}$$

The anisotropy decay was fitted with a model function comprising a sum of three exponentials as well as with Eq. 6.

Molecular dynamics simulations

Three simulation systems were constructed. The first two systems contained one Alexa488 dye molecule (see *inset* of Fig. 3) solvated in methanol and
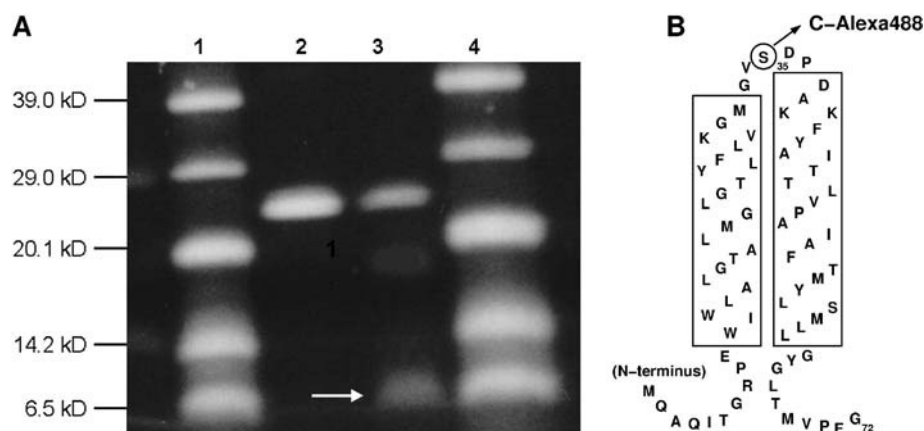
FIGURE 2 (*A*) SDS-PAGE of fluorescently labeled bacteriorhodopsin S35C-Alexa488. (Lanes *1* and *4*) Molecular weight marker, (lane *2*) undigested bacteriorhodopsin S35C-Alexa488, (lane *3*) partially digested bacteriorhodopsin S35C-Alexa488. The AB fragment in lane *3* is marked by a white arrow. (*B*) Secondary structural model of the AB-helix fragment of bacteriorhodopsin. The amino acids are shown in single letter code.

water, respectively. The third system comprised the AB fragment of bR with the Alexa488 dye attached to position S35C, solvated in methanol. All MD simulations were performed using the GROMACS simulation software (31) with the united-atom GROMACS force field, which describes nonpolar hydrogens implicitly via compound atoms. The compound atom approximation could potentially underestimate C-H/aromatic interactions between the protein and the dye. However, we do not expect this effect to significantly influence our results. The SPC (32) water model was used. The methanol parameters were taken from the GROMACS force field. The force-field parameters for the dye have been determined as described below. All systems were energy minimized to obtain the starting configuration for the simulations. Periodic boundary conditions were applied. In the free-dye simulations the solvent and the solute were jointly coupled to an external temperature bath of 300 K with a relaxation time of 0.1 ps (33). For the protein-dye system the solvent was separately coupled to a heat bath with the same parameters. In all simulations the system was weakly coupled to a pressure bath of 1 atm with isotropic scaling and a relaxation time constant $\tau_p = 1$ ps. Bond lengths were constrained to their equilibrium lengths using the LINCS algorithm (34). This allowed for a 2-fs time step using the leapfrog integration scheme. For the Lennard-Jones interactions, a cutoff distance of 1.0 nm was applied. Electrostatic interactions between charge

groups at a distance $<$1 nm were calculated explicitly, and the long-range electrostatic interactions were calculated using the particle-mesh Ewald method (35) with a grid spacing of 0.12 nm and a fourth-order spline interpolation. Coordinates of all atoms were saved every 1 ps for further analysis. The initial structure of the AB fragment (residues 8–71) of bacteriorhodopsin was taken from the crystal structure, Protein Data Bank entry 1AP9 (36). It has been shown that the AB fragment solvated in an organic solvent (methanol/chloroform (1:1)) adopts a conformation similar to its structure in bR (37).

Parameterization of the dye

Because the motional restriction of the dye due to the protein surface is mainly determined by steric hindrances and electrostatic interactions, we paid particular attention to those force-field parameters that sensitively affect these quantities, i.e., van der Waals parameters and partial charges. The van der Waals parameters are relatively insensitive to the chemical environment and were thus taken from corresponding atom types from the GROMACS force field. For the aliphatic linker region, parameterization was straightforward because this region is chemically sufficiently similar to aliphatic groups in the GROMACS force field. Similarly, the force constants describing the
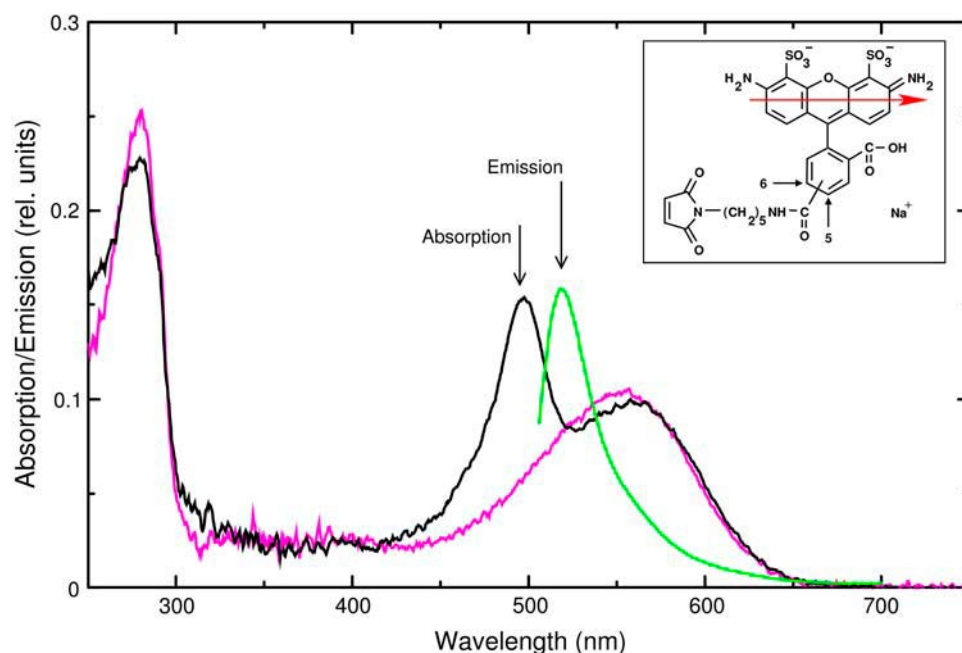

FIGURE 3 Absorption (*black*) and emission (*green*) spectra of the fluorescent dye Alexa488 covalently bound to a single cysteine on the surface of bacteriorhodopsin in position 35. The absorption spectrum unlabeled bacteriorhodopsin (*pink*) is shown for comparison. The spectra are scaled. The absorbance and emission maxima of Alexa488 are marked. The labeling stoichiometry Alexa/bR was 0.63. Conditions are: 0.1% CHAPS, 150 mM KCl for the absorbance spectra; methanol for the fluorescence emission spectrum of the fragment (1–72) S35C-Alexa488. The inset shows the chemical structure of Alexa488; the arrow indicates the transition dipole moment of the chromophore.

chemical bonds within the headgroup of the dye have been adapted from the GROMACS force field. Due to the extended π-electron system of the dye, this simple estimate is not expected to yield accurate force constants; however, as the internal vibrations of the dye are largely uncoupled from the overall diffusive dye motion of interest, this inaccuracy is not expected to affect our results. For the free dye, this assumption has been verified by test simulations with varying force parameters (data not shown).

The partial charges for the dye headgroup are critical and therefore have been determined from QM calculations. In all QM calculations described below, only the headgroup of the dye is considered, with the linker replaced by a methyl group. Here, the calculation is complicated by the fact that, to simulate the experiment properly, the molecular dynamics between absorption and emission have to be studied. Therefore, the dye parameters have to be determined for the first excited state.

To that aim, we followed a hybrid strategy. In a first step, the ground state of this molecule was calculated using density functional theory (DFT) as implemented in the DMol program (38) with the DNP basis set and the BLYP functional. Then both the ground and first excited states were calculated using CIS/STO-3G with the GAUSSIAN program (ab initio) (39) and also, as a check, at the semiempirical level PM3 with the program MOPAC (40). Atomic charges from all calculations were obtained by fitting to the electrostatic potential (''ESP charges'') (41). The differences of the charges between the ground and first excited state obtained from the ab initio and semiempirical calculations were small; we therefore took their mean values to minimize the complementary systematic errors inherent to both methods. These differences were then added to the ground-state DFT charges. To assure compatibility to the GROMACS protein force field, partial charges for all 20 amino acids were calculated using the same DFT level. From comparison to the respective GROMACS partial charges, a mean scaling factor of 0.7 was obtained and applied to the dye charges, including a shift to retain the correct total charge of $-2e$. Finally, the slightly unsymmetric charges were symmetrized, according to the symmetry of the dye, to resemble the ensemble average in a mean field approach. Force-field parameters of the bond lengths and angles were obtained from the ab initio geometry calculation.

The Alexa488 (Molecular Probes) dye is only available as a mixture of 5- and 6-isomers (cf. *inset* of Fig. 3); we restricted our simulations to the 5-isomer, assuming only minor dependence of the dye dynamics on the choice of the isomer. The parameter files for this dye can be downloaded from our website (http://www.mpibpc.gwdg.de/groups/grubmueller/probflex/).

Probability distribution of the dye from a vacuum simulation

For efficient sampling of the conformational space of the dye, simulations at 1000 K with implicit solvent were carried out. The central oxygen atom in the headgroup of the dye (cf. *inset* of Fig. 3) was chosen to represent the conformation of the dye, and the probability distribution p_{high} of this atom at high temperature was obtained from the simulation. Because the equilibrium distribution of the dye is predominantly governed by the electrostatic interactions between the dye and the protein, this interaction was calculated for each conformation visited in the simulation. To account for the dielectric properties of the thin methanol layer between the dye and the protein, we derived a corrected dielectric coefficient by scaling a distance-dependent dielectric coefficient obtained for water (42). Following this approach, and using the distance between the dye and the protein of ~ 0.5–0.8 nm as observed in the simulation, a dielectric coefficient of $\epsilon = 10$ was obtained and used for the calculation of the electrostatic energy. This energy $E_{Coulomb}$ served to estimate the probability distribution p at room temperature from the high temperature distribution p_{high} via the Boltzmann factor,

$$p \propto \exp\left[-\left(E_{Coulomb} - k_B T_{high} \ln p_{high}\right)/(k_B T)\right], \quad (9)$$

with $T_{high} = 1200$ K and $T = 300$ K. We note that the obtained probability distribution p (Fig. 7 *C*), is expected to provide only a rough estimate.

Certainly, solvent effects will not fully be described by the implicit solvent treatment, which was necessary to obtain sufficient sampling.

Correlation analysis

The correlation between the dye and the protein was calculated using a modified version of the LMLA (localized mean by linear assignment) algorithm (43). This algorithm serves to obtain curvilinear principal coordinates from molecular ensembles of conformations, represented as sets of points $\mathbf{x}^{(i)}$ in the $3N$-dimensional configurational space of an N-atomic molecule. The main idea of this approach is that a large number of randomly chosen k-tuples of structures probe the shape the molecular ensemble and, therefore, by properly averaging over all these k-tuples, information on the ''average shape'' of the whole ensemble can be obtained. This information is represented in terms of k ''prototypic structures'' (PS) in the conformational space, which are positioned along the largest extension of the molecular ensemble, thus capturing the main conformational changes of the system.

The PS $\mathbf{a}_j$ are calculated as localized ensemble averages

$$\mathbf{a}_j = \langle \mathbf{x}^{(i)} \rangle_{S_j}, \quad (10)$$

where the localization is introduced by restricting the ensemble average to sets S_j of structures, which are defined by the assignment condition

$$\sum_{j=1}^{k} |\mathbf{a}_j - \mathbf{x}^{(i)}|^2 \stackrel{!}{=} \min, \ \forall \, \mathbf{x}^{(i)} \in S_j, \quad (11)$$

further requiring that each S_j contains the same number of elements and that for each $\mathbf{x}^{(i)}$ there must be exactly one j for which $\mathbf{x}^{(i)} \in S_j$.

Here we are not interested in a description of the conformational changes of the whole system, i.e., dye and protein. Rather, we wish to analyze which motions of the protein are probed by the motion of the dye attached to it, i.e., which collective mode of motion is best correlated with the configurational subspace defined by the dye. To this aim, the LMLA algorithm is modified such that the linear assignment of Eq. 11 is done only within the subspace of the dye coordinates,

$$\sum_{j=1}^{k} |\mathbf{P}\tilde{a}_j - \mathbf{P}\mathbf{x}^{(i)}|^2 \stackrel{!}{=} \min, \ \forall \, \mathbf{x}^{(i)} \in \tilde{S}_j, \quad (12)$$

where $\mathbf{P}$ is the projector onto the subspace of the dye. The new PS $\tilde{a}_j$ are obtained as in Eq. 10,

$$\tilde{a}_j = \langle \mathbf{x}^{(i)} \rangle_{\tilde{S}_j}, \quad (13)$$

and will be referred to as subspace-determined PS to distinguish them from the complete-space-determined PS obtained from the conventional LMLA algorithm. As is shown in more detail by Schröder (43), the subspace-determined PS are indeed positioned along the direction in the conformational space, which is best correlated with the motion of the dye. We note that the LMLA algorithm is a generalization of the principal component analysis (PCA) to curvilinear coordinates (43).

Here, $k = 3$ was found to describe the nonlinear motions of interest sufficiently accurately; therefore, three subspace-determined PS (conformations of the dye-protein system) were calculated from the ensemble generated by the explicit solvent MD simulation at 300 K.

To quantify the contribution of each single protein atom to the obtained correlation with the dye, we calculated the root mean square fluctuation (*rmsf*) σ_i of the obtained $\tilde{a}_j$ for each atom i,

$$\tilde{\sigma}_1 = \sqrt{\frac{1}{k}\sum_{j=1}^{k} |\tilde{a}_{j,1} - \langle \tilde{a}_{j,1} \rangle_j|^2}, l = 1, \ldots, N, \quad (14)$$

for each 3-vector $\tilde{a}_{j,l}$ pertaining to atom l. Because this measure $\tilde{\sigma}_l$ would include both the correlation of interest as well as the fluctuation of the

protein atom (which does not contain information on any correlated motion), the influence of the latter was removed by considering $c_1^2 = \tilde{\sigma}_1^2 - \sigma_1^2$ as the pure (relative) correlation measure. These values are depicted color coded in Fig. 10.

Analysis of depolarization timescales

To characterize the fluorescence anisotropy decay on different timescales, we calculated a position-dependent contribution to the depolarization of the dye. To this aim, only five degrees of freedom of the dye trajectory were considered: The position of the dye, represented by the center of mass $\mathbf{x}_m$ of the headgroup of the dye, and the normalized vector of the transition dipole moment $\boldsymbol{\mu}(t)$. To gain information on the timescale of the respective correlations, we compared the original MD trajectory to a smoothed trajectory, where the fast fluctuations were filtered out and only the slow components of the dye dynamics remained. Only the transition dipole vector was low-pass filtered (yielding $\boldsymbol{\mu}_s(t)$) using a Gaussian kernel with a mean ± SD σ = 40 ps, whereas the $\mathbf{x}_m$ trajectory remained unchanged.

To obtain a spatially resolved picture, the contributions $\xi(t') = P_2[\boldsymbol{\mu}(t') \cdot \boldsymbol{\mu}(t' + t)]$ to the anisotropy $r(t)$ at $t = 50$ ps (cf. Eq. 2) were calculated. The position-dependent contribution to the depolarization $\tilde{\xi}(\mathbf{x})$, which is a measure for the orientational flexibility at a given position $\mathbf{x}$ of the dye, is then obtained by

$$\tilde{\xi}(\mathbf{x}) = \frac{\sum_t \xi(t) \exp[-(\mathbf{x} - \mathbf{x}_m(t))^2/(2\rho^2)]}{\sum_t \exp[-(\mathbf{x} - \mathbf{x}_m(t))^2/(2\rho^2)]}, \qquad (15)$$

with $\rho = 15$ Å, chosen to trade off smoothness and resolution. The same calculation was also done for the smoothed trajectory $\boldsymbol{\mu}_s(t)$, yielding the corresponding function $\tilde{\xi}_s(\mathbf{x})$.

Orientation distribution of the dye

The orientation distribution (cf. Fig. 14), represented as a histogram on the surface of a sphere, has been built up of 500 cones pointing away from the average center-of-mass position of the headgroup of the dye. Their orientation is defined by 500 randomly chosen unit vectors. Their lengths n_j represent the number of transition dipole orientations that fall into the respective directions,

$$n_j = \sum_{i=1}^n \exp[|\mathbf{r}_i \cdot \mathbf{g}_j|/(2\sigma^2)], \qquad (16)$$

using a variance $\sigma^2 = 0.025$, where n is the number of frames of the trajectory (10,000 for conformation A, 5000 for B), and $\mathbf{r}_i$ is the normalized transition dipole vector of the i-th frame. For the graphical representation, the lengths of the cones were shifted and scaled such that they covered the range 5.0–8.5 Å.

To assess the orientational distribution of the dye in conformation A within the loop frame, all structures from the trajectory were aligned to minimize the root mean square deviation *rmsd* of the loop residues 30–42. For the distribution in conformation B, all structures were aligned to minimize the *rmsd* of the helical residues (10–29,43–61).

Calculation of the fluorescence anisotropy from the simulation

The anisotropy decay $r(t)$ due to the change in the orientation of the transition dipole moment of the dye between absorption and emission has been calculated according to Eq. 2. To this aim, the time-dependent absorption and emission dipole moments, $\boldsymbol{\mu}_a(t) = \mathbf{M}(t) \cdot \boldsymbol{\mu}_a$ and $\boldsymbol{\mu}_e(t) = \mathbf{M}(t) \cdot \boldsymbol{\mu}_e$, had to be derived from the MD simulations. Here, $\boldsymbol{\mu}_a$ and $\boldsymbol{\mu}_e$ are the dipole moment

vectors in the coordinate frame of the moving dye and $\mathbf{M}(t)$ is a rotation matrix that transform the dye coordinate frame into the lab frame. The absorption dipole moment $\boldsymbol{\mu}_a$ in the dye frame has been obtained from the CIS calculation of the dye described above and is oriented along the three-ring system of the chromophore as shown in the inset of Fig. 3 (*arrow*). The rotation matrix $\mathbf{M}(t)$ is calculated for each snapshot of the MD trajectory (in 1-ps steps) from the instantaneous structure of the dye, thus yielding a trajectory of the absorption dipole vector $\boldsymbol{\mu}_a(t)$. The emission dipole moment in the dye frame, $\boldsymbol{\mu}_e$, was not calculated explicitly. Rather, the angles $\lambda = 10°$ and $\lambda = 13°$ between $\boldsymbol{\mu}_a$ and $\boldsymbol{\mu}_e$ were determined from the measured initial anisotropies $r_0 = 0.37 = 0.4 P_2(\cos \lambda)$ and $r_0 = 0.34$ for the label free in solution and for the label-loop construct, respectively, and found to be small. In this case, λ enters into $r(t)$ as an overall scaling factor, and thus the normalized decay curve studied here is not affected. Therefore, $\boldsymbol{\mu}_e(t)$ was replaced by $\boldsymbol{\mu}_a(t)$.

Statistical accuracy of calculated anisotropy decay

The time average used to calculate the anisotropy decay $r(t)$ (cf. Eq. 2), obtained from one trajectory, implies a statistical error. To estimate this error, Brownian dynamics simulations have been carried out for the cone-in-a-cone model. In these simulations, 230 rotational diffusion trajectories of a single normalized vector, representing the transition dipole moment of the dye within the dye cone, as well as the diffusion of the dye-cone axis within the protein cone have been calculated. The lengths of these trajectories (16 ns) have been chosen identical to the length of the MD trajectory of the full dye-protein system. The rotational diffusion coefficients and semicone angles for the dye and the protein cone (0.0018 ps^{-1}, 0.0003 ps^{-1} and 45°, 50°, respectively) were chosen such as to match those extracted from the MD simulation (Table 1). From each of these 230 trajectories $r(t)$ has been calculated as described above, and for each $r(t)$, cone-in-a-cone parameters were obtained. From their variances, the statistical error of the cone-in-a-cone parameters derived from the MD simulation was estimated (Table 1).

RESULTS AND DISCUSSION

Rotational diffusion of a free dye in methanol and water

In a first step, we studied if and to what extent MD simulations allow us to predict the fluorescence anisotropy of a dye and if the used dye and solvent force-field parameters are accurate enough for this purpose. To this aim, simulations of the free dye in methanol and water were carried out and the fluorescence anisotropy calculated from the simulations was compared to experiment. The Alexa488 dye was used both in the experiment described further below, as well as in the simulations.

One Alexa488 molecule was simulated in a box of 4673 water molecules for 8 ns and in a box of 1317 methanol molecules for 13 ns. The dye was free to undergo translational and rotational diffusion within the (periodic) simulation volume. Fig. 4 *A* shows the calculated anisotropy as solid lines (*green*, methanol; *blue*, water). Fits to a single exponential function yield a rotational correlation time of $\phi = 51$ ps for the dye in water and $\phi = 86$ ps in methanol. Fig. 4, *B* and *C*, show the measured time-resolved fluorescence intensities of Alexa488 in aqueous solution and in methanol at 300 K. The corresponding anisotropy decay curves, calculated from
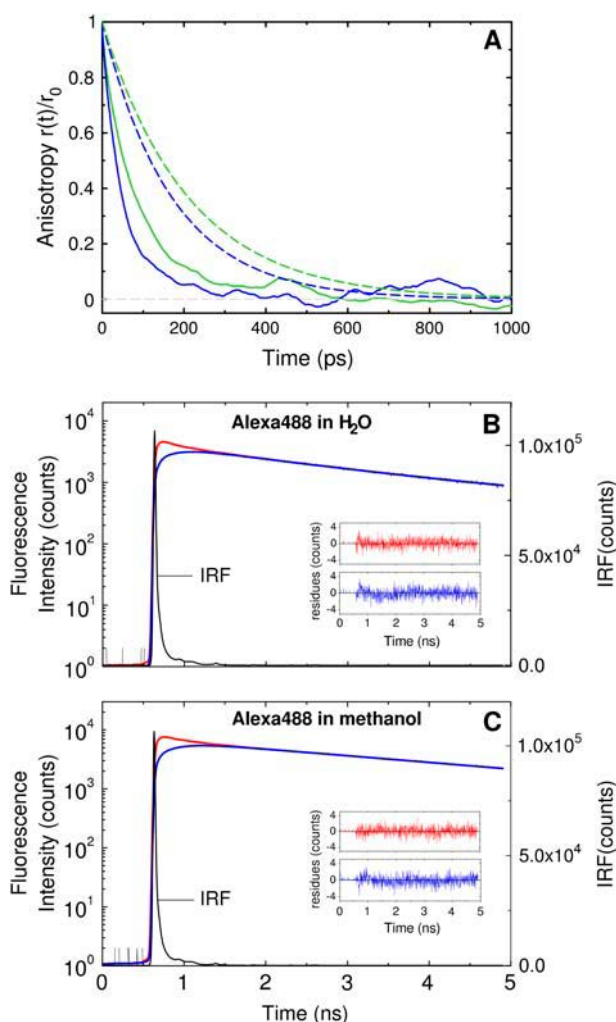
FIGURE 4 (A) Calculated fluorescence anisotropy decays (*solid lines*) for Alexa488 in water (*blue*) and methanol (*green*) are compared to the measured anisotropy decays (*dashed lines*). (B and C) Time courses of the fluorescence intensities $I_\parallel(t)$ (*red*) and $I_\perp(t)$ (*blue*) in water (B) and methanol (C). IRF is the instrument response function. The residuals of the fit for $I_\parallel(t)$ and $I_\perp(t)$ are shown as insets. The excitation was at 470 nm. The fluorescence emission was detected after passing through a cutoff color glass filter OG 515.

the two components of fluorescence decay $I_\parallel(t)$ and $I_\perp(t)$ according to Eq. 1, are shown as dashed lines in Fig. 4 A. The fluorescence lifetime in water was fitted with two exponentials, $\tau_1 = 1.97 \pm 0.03$ ns and $\tau_2 = 8.68 \pm 0.03$ ns and the anisotropy decay was fitted with one exponential, yielding a rotational correlation time $\phi = 170$ ps. The fluorescence lifetime and the anisotropy decay of Alexa488 in methanol were fitted with single exponentials, $\tau = 3.82 \pm 0.02$ ns and $\phi = 210$ ps, respectively. The residuals of the fit for $I_\parallel(t)$ and $I_\perp(t)$ are shown as insets in Fig. 4, A and B, respectively. The final χ^2 of the fit was 1.02 for Alexa488 in water and 1.007 in methanol. *IRF* is the instrument response function with a full width at half maximum of 48 ps.

As can be seen, the correlation times in the simulation are smaller than in the experiment by about a factor of 3. Further studies (43) suggested this effect to be due to the solvent force fields. In particular, self-diffusion coefficients and dielectric relaxation times of solvent molecules obtained from MD simulations were compared to experiment and found to deviate systematically from each other. This deviation could explain the too-fast rotational diffusion of the dye molecule in the simulation. Nevertheless, the details of this effect are not fully understood yet and need to be further investigated.

Both, in the simulation as well as in the experiment the dye shows faster rotational diffusion in water than in methanol. This behavior was unexpected because the viscosity of water (1.002×10^{-3} Pa s (at 293 K)) is larger than that of methanol (0.587×10^{-3} Pa s (at 293 K)). Furthermore, a similar experiment with fluorescein dyes shows the normal behavior; with measured rotational correlation times of 140 ps in methanol and 170 ps in water (data not shown).

To explain this inverse solvent effect for Alexa488, the structure of the dye in the simulation was analyzed in more detail. Visual inspection suggested that the extension of the dye strongly depends on the solvent. Fig. 5 C quantifies this extension by the distance d defined in Fig. 5 A, for both simulations in methanol (*green curve*) and water (*blue curve*). As can be seen, d fluctuates between 0.7 and 1.6 nm. The representative dye conformations are shown in Fig. 5, A and B, for $d = 1.6$ nm and $d = 0.7$ nm, respectively. As the structures show, the headgroup of the dye is rather stiff, thus the change of the length is only due to the flexible linker, a hydrophobic chain. The average length of the dye in methanol of ~1.5 nm is clearly larger than that in water of ~1.0 nm (*thick horizontal lines*).
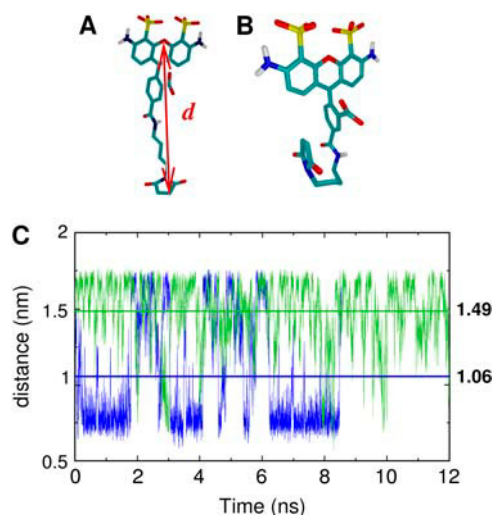

FIGURE 5 Extension of the Alexa488 dye molecule solvated in water and in methanol, as quantified by the distance d defined in panel A (*arrow*). This distance is plotted versus time for the water (*blue*) and methanol (*green*) simulations. (B) Dominant conformation of the dye solvated in water, with a distance $d = 0.8$ nm.

This observation can be explained in terms of the water-exposed hydrophobic surface. In water, the hydrophobic chain minimizes the water-accessible surface by coiling up and thereby reducing the effective size of the molecule. In the more hydrophobic solvent, the hydrophobic forces are absent, and the chain remains in the entropically more favorable extended conformation. We suggest this as an explanation of the observed faster rotational diffusion of Alexa488 in water than in methanol. Furthermore, the lack of this flexible hydrophobic chain in fluorescein explains, why in this case this inverse solvent effect was not observed. These results show that the simulations of the dye are capable of describing the subtle difference in the rotational diffusion of the dye solved in water and methanol.

Dye conformations on the bR surface in the simulation

Having passed these initial tests, we simulated the Alexa488 dye attached to the S35C position of the AB-helix fragment (residues 8–71) of bR solvated in 18,752 methanol molecules and including two sodium ions for 26 ns. Fig. 6 shows the *rmsd* of the backbone atoms of the helical part (residues 10–29 and 43–61). The *rmsd* reaches a relatively low mean *rmsd* value of 0.12 nm after only ~20 ps, which indicates that the α-helical structure remains very stable during the simulation. Furthermore, the root mean square fluctuation (*rmsf*) around the mean structure of ~0.02 nm indicates a low flexibility of the protein. In contrast, the loop connecting the two helices shows a much higher flexibility than the helical regions, which will be discussed further below.

The initial dye geometry was chosen in extended conformation, detached and pointing away from the surface. After ~500 ps, the dye reached conformation A, shown in Fig. 7 *A*, and remained loosely bound via noncovalent interactions
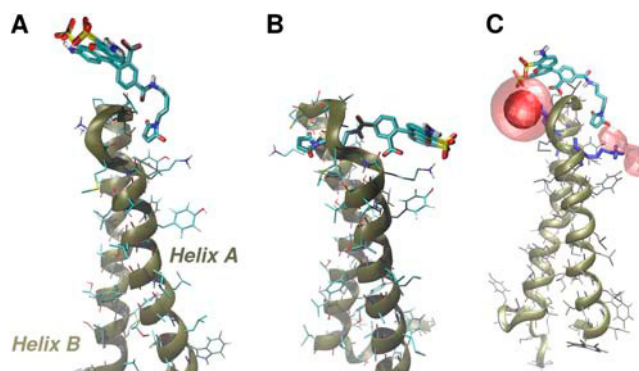
FIGURE 7 Snapshots of the bR protein fragment with covalently bound dye in different conformations (*side view*), as obtained from the MD simulation. During the first 16 ns, the dye adopts conformation A (*A*) and is highly mobile. For the rest of the simulation, the dye remains in conformation B (*B*) and is much less flexible, as it is more tightly attached to the two helices. (*C*) The probability distribution of the dye calculated from the vacuum simulations *p* is visualized by red isosurfaces on two different contour levels, which enclose 60 and 90% of the probability density (solid and transparent surfaces, respectively).

to the protein surface. It then detached from the surface and flipped back toward the other side into conformation B, shown in Fig. 7 *B*, where it remained for the rest of the simulation. In conformation B, the dye is much less flexible than in A, as quantified by the *rmsf* of 0.15 and 0.23 nm, respectively. In conformation A, the dye adopts two conformational substates, shown in Fig. 8 ("up" and "down"). During the residence time of 16 ns in conformation A, the dye flipped back and forth three times between these two substates, which significantly contributes to the mobility of the dye. This complex and hierarchical motion is apparently insufficiently described by a simple wobbling-in-a-cone model.

Unfortunately, the occupancy of conformations A and B cannot be directly inferred from the simulation, because only one transition was observed. As a substitute for this lack of reversibility during the simulation time, high-temperature vacuum simulations were carried out to sample the conformational space of the dye more efficiently. From these simulations, a room temperature probability distribution *p* of the dye positions based on the electrostatic dye-protein interactions was derived, as described in Methods. Fig. 7 *C* shows two isosurfaces of *p* in red enclosing 60 and 90% of the probability density, respectively. Qualitatively, as can be
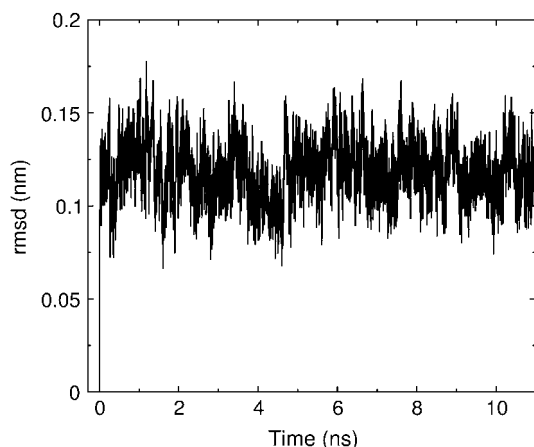

FIGURE 6 Root mean square deviation (*rmsd*) of the backbone atoms of the helical residues (residues 10–29 and 43–61) from the initial x-ray structure during the first 10 ns of the simulation.
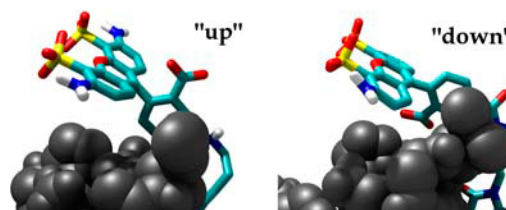

FIGURE 8 Transitions of the dye between two subconformations "up" and "down" of conformation A on the nanosecond timescale. The restriction of the mobility of the dye in both conformations is quite similar.

seen from the figure, the dye is in conformation A more often than in B. This is mainly due to the favorable electrostatic interactions between the dye and the protein: In conformation A, the negatively charged dye has contact to two lysines (colored *blue* in Fig. 7 C), whereas in conformation B it only has contact to one lysine. In addition, as will be described further below, the calculated fluorescence anisotropy of the dye in conformation A agrees much better with the measured one than it does in conformation B. Thus, we assume that conformation A is the dominant conformation of the dye.

Influence of the dye on loop flexibility

To address the question if and to what extent the dye influences the protein conformation and dynamics, we compared a 5-ns part of the simulation described above to a 5-ns simulation of the same system without the dye. We focused on the change in the flexibility of the protein and in particular of the loop region, where the dye is attached. The flexibility is quantified by the *rmsf* of the backbone, shown in Fig. 9 for the protein with bound dye (*dotted line*) and without the dye (*solid line*). For the calculation of the *rmsf* the trajectory was fitted onto a reference structure using only the helical residues to focus the analysis on the loop region (*thick solid bar*). As can be seen, the overall shape of both curves is quite similar. Only the loop residues show a slight decrease of the flexibility, whereas the rest of the protein is hardly affected by the dye. But also for the loop region, the attached dye decreases the *rmsf* only by maximally 15%. Therefore, the assumption necessarily made for all spectroscopic measurements of this kind, that the dye does not severely influence protein dynamics is, at least for this case, justified.

Dye-protein correlation

With these results at hand, we can now address the question of which protein region or, more precisely, the motion of

which protein region is actually probed by the dye. To this aim, we quantified the correlation between protein and dye motion, as described in Methods and shown color-coded in Fig. 10. Those residues that show the largest correlations (*red*) are, therefore, those which are ''seen'' via the dye. Note that the obtained measure of correlation is only a relative one.

The highest correlations are seen for residues Gly-33 and Val-34, which are next to the Cys-35 residue to which the dye is covalently bound (Fig. 10, *bottom*, *black curve*). These highly correlated residues are in close vicinity to the dye headgroup and also form frequent sterical contacts to the dye. Accordingly, they transmit their high flexibility via noncovalent interactions to this headgroup containing the chromophore of the dye molecule, which is observed in the experiment. Comparison of this correlation with the mean square fluctuation (*msf*) of the involved residues (Fig. 10, *bottom*, *blue curve*), shows that the motion of the dye is mainly governed by the more flexible part of the loop,
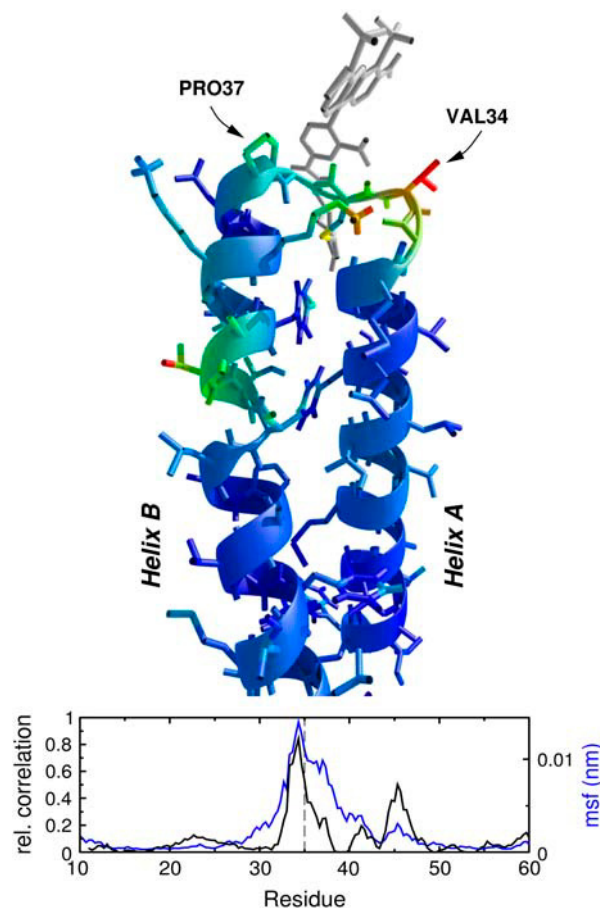
FIGURE 10 One Alexa488 dye molecule attached to the loop of the bR fragment. The protein is colored according to the relative correlation (arbitrary units) of its motion with the motion of the dye. High (low) correlations are shown in red (*blue*). The bottom panel shows the relative correlation (*black line*) and the mean square fluctuation (*msf*; *blue line*) of the protein backbone.
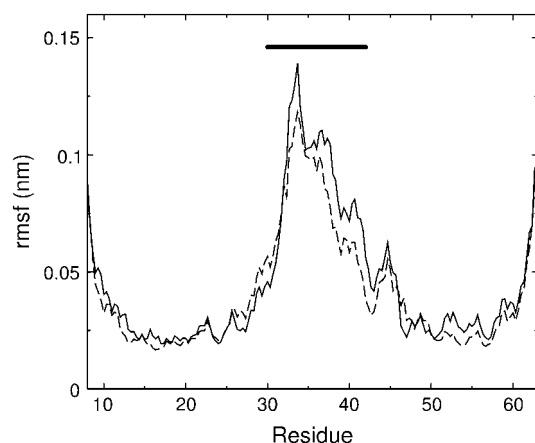

FIGURE 9 Root mean square fluctuations (*rmsf*) of the protein backbone for the protein with the bound dye (*dotted line*) and without the dye (*solid line*). The thick solid bar on top denotes the loop residues.

residues 33 and 34. This agrees with the general expectation that mainly the more flexible residues contribute to the fluorescence depolarization. From this follows that depolarization experiments do not necessarily probe only the residue to which the dye is attached, but rather the flexibility of an entire segment—in our case, the flexible region comprising residues (33–37). Also, the region around residue Ile-45, in the middle part of the left helix (helix B) in Fig. 10, shows a significant correlation, whereas the helix connecting this residue to the loop does not show any correlation. This is remarkable and shows how correlated motions can be transmitted via larger helix parts, e.g., necessary for signal transduction in GPCRs. Here, relatively small correlated motions of the helix induce larger correlated motions in residue 45.

One main goal of this work, as mentioned above, was to identify the kinetic component in the anisotropy decay $r(t)$ of the dye that is governed by and, hence, yields information about, the protein dynamics. To this aim, the reorientational dynamics of the transition dipole moment of the dye was studied. To correlate it with the protein dynamics studied above, the orientational dynamics was analyzed and quantified as a function of dye position, as described in Methods. Fig. 11 A shows the obtained map, viewed from the bottom side with the protein backbone superimposed; the color encodes the contribution $\tilde{\xi}(\mathbf{x})$ to the depolarization decay at 50 ps. This period was chosen as a tradeoff between spatial resolution—the dye should not move too far during this period—and sufficient reorientation.

As can be seen, $\tilde{\xi}(\mathbf{x})$ is nearly uniform throughout the region covered by the dye. Here, the fast reorientational dynamics of the dye dominate possible—and presumably slower—components that could correlate with the protein motions. These have therefore been filtered in Fig. 11 B,
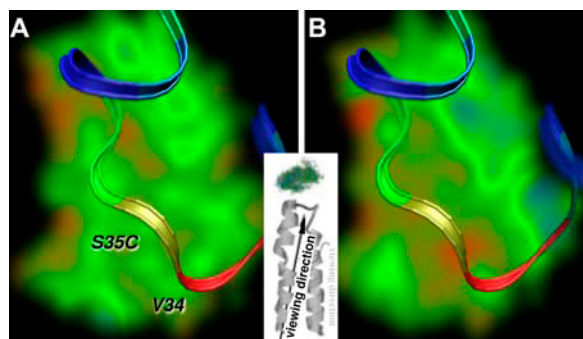
which was derived similarly as Fig. 11 A, but using a smoothed trajectory, for which fast fluctuations have been suppressed. The smoothing filter has been chosen to suppress the fastest decay (120 ps) within the decay curve calculated from the trajectory as described in Methods; thus, the decay curve calculated from the smoothed trajectory lacks the 120-ps component, but still contains components slower than 300 ps.

Indeed, the obtained map $\tilde{\xi}_s(\mathbf{x})$ shows high orientational mobility (*red*) near the loop region with a maximum close to residues 33 and 34, which have been identified above to move strongly correlated with the dye. In contrast, for distant dye positions, its orientational dynamics is less pronounced (*blue*) and, therefore, contributes little to the observed depolarization. We conclude that there is a slow component of the dye dynamics, which is correlated with the protein motion and which is slower than 300 ps.

Comparison of experiment and simulation

In the measured curve, shown in Fig. 12 A, three decay components can be resolved: two faster components ($\phi_1 =$
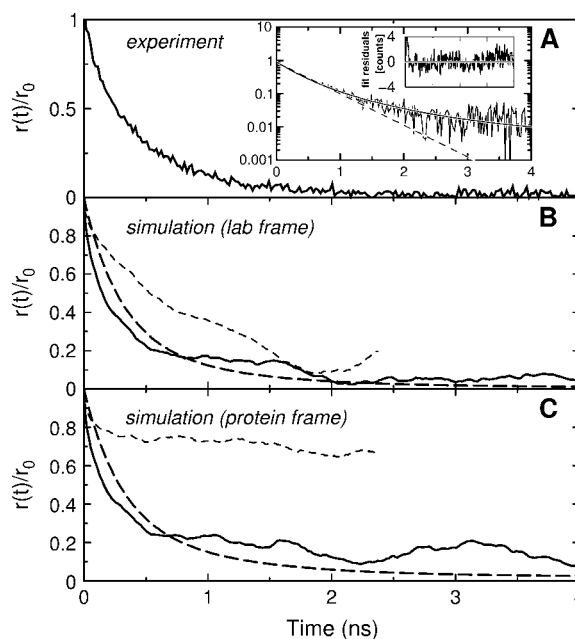

FIGURE 11 Analysis of the timescale of the dye-protein correlation. The inset shows the viewing direction used in panels A and B. The ribbons in the foreground depict the protein backbone looking upwards from the bottom of the protein. The backbone is colored according to the correlation of the protein motion with the dye motion, as in Fig. 10. The ''cloud'' in the background shows all the positions that are visited by the center of mass of the dye headgroup during the simulation. The coloring of this ''cloud'' denotes the contribution to the depolarization via its orientational mobility. Red, green, and blue indicate high, mid-, and low mobility of the dye, respectively. This coloring has been calculated from the original (A) and from a smoothed (B) trajectory.

FIGURE 12 Anisotropy decay curves from simulation and experiment, normalized by the initial anisotropy r_0. (A) Measured anisotropy decay (convoluted with the instrument response function). The inset shows a logarithmic plot of this curve together with the residuals of the fit to Eq. 6. (B) Anisotropy of the dye in conformation A (*solid line*) and in conformation B (*short dashes*) calculated from the MD trajectory. Also shown (*long dashes*) is the fit curve of the cone-in-a-cone model to the experimental curve, using the parameters shown in Table 1. (C) Anisotropy in the protein frame for conformation A (*solid line*) and for conformation B (*short dashes*), calculated from a trajectory that has been fitted onto a reference structure. The long-dashed line shows the same fit curve as in panel B, except with the global rotational correlation time ϕ_G set to infinity. This curve thus corresponds to the measured anisotropy in the protein frame.

296 ps and $\phi_2 = 805$ ps) are assumed to arise from the dye motion relative to the protein (8), where the slower of these two components is suggested to be influenced by the local protein flexibility, as analyzed in the previous section. The third (slowest) component of 5 ns originates from the overall tumbling motion of the protein-dye complex. To visualize these multiple decay components, the inset in Fig. 12 *A* shows a logarithmic plot of the anisotropy decay and the corresponding fit curve. The measured anisotropy decay curve has been additionally fitted using the cone-in-a-cone model (Eq. 6); the resulting parameters are shown in Table 1 (Experiment).

Anisotropy decay curves have been calculated from the simulation, as described in Methods. Separate curves have been calculated for the dye in conformation A and B, shown in Fig. 12 *B* as solid and short dashed lines, respectively. As discussed above, for the comparison of the anisotropy with the experiment, the first 16 ns of the simulation have been used, during which the dye is in conformation A. Because the overall tumbling motion of the dye-protein system is not of interest here, this motion has been suppressed by least-square fitting all protein structures to a reference structure. The resulting trajectory, thus, describes the dye dynamics in the coordinate frame of the protein. Fig. 12 *C* shows the obtained anisotropy decay. Also this decay curve was fitted to the cone-in-a-cone model (Eq. 6), setting $\phi_G = \infty$, and thereby also suppressing global rotational diffusion. The decay parameters obtained from this fit (A_1, ϕ_1, A_2, and ϕ_2) are shown in Table 1 (Simulation).

Fig. 12 *C* shows that the anisotropy of the dye in conformation B (*short dashed line*) is significantly higher than in conformation A (*solid line*), as discussed above. Additionally, the elimination of the overall tumbling allows for a fit using two instead of three exponentials (cf. Eq. 6), which significantly improves the accuracy of the obtained decay parameters for the local motion of the dye. Because the internal protein and dye dynamics can be assumed to be uncoupled to the overall rotational diffusion, we prefer to compare with experiment the parameters obtained from Fig. 12 *C*, i.e., from the more reliable fit.

Considering the systematic acceleration of simulated rotational diffusion, which is, as can be seen, comparable to the acceleration of the free dye analyzed above, the agreement of the fit parameters (Table 1) between experiment and

simulation is sufficiently good to assign decay components properly. In particular, the amplitude A_1, which describes the dye-cone angle in the cone-in-a-cone model, matches quite well, indicating that the simulation accurately describes the local wobbling of the dye. The second amplitude A_2 will be analyzed in more detail further below.

The rotational correlation time ϕ_G of the global rotation of the protein was obtained from the experiment, as described above, by fitting the cone-in-a-cone model (Eq. 6) to the anisotropy decay. From the simulation $\phi_G = 3.9$ ns was obtained via $\phi_G = 1/(6D_G)$ from the rotational diffusion coefficient of the protein $D_G = 4.3 \times 10^{-5}$ ps^{-1}, in good agreement with the experimental value of 5 ns.

Statistical error of the decay parameters

The limited length of the calculated trajectory (16 ns) causes a statistical error for the average (Eq. 2) in the calculation of the anisotropy decay, and therefore also in the fitted cone-in-a-cone parameters (44). The straightforward approach to estimate this error would be to calculate many similar MD trajectories and to analyze the variance of the decay parameters obtained from each of the trajectories. Unfortunately, the calculation of just one trajectory required already four months of computer time, so this option is not practicable.

Instead, we used an approach, which is principally the same as the one suggested before, but differs in the way the trajectories are obtained. Assuming the dye dynamics to be sufficiently well described by the cone-in-a-cone model, the many required MD simulations are substituted by Brownian dynamics simulations of the transition dipole moment diffusion in the cone-in-a-cone model. From these Brownian dynamics simulations, 230 trajectories were obtained, from which 230 anisotropy decay curves were calculated. By fitting the cone-in-a-cone model, Eq. 6, to these curves, 230 decay parameter sets were obtained. Their variances serve as a measure of the expected statistical errors.

The error of the fast rotational correlation time, $\Delta\phi_1 = 5$ ps, is significantly smaller than that of the slow correlation time, $\Delta\phi_2 = 120$ ps, because the larger rotational diffusion coefficient yields better sampling of the dye cone. The errors of the amplitudes, $\Delta A_1 = \Delta A_2 = 0.02$, imply errors of the semicone angles of $\Delta\theta_1 = \Delta\theta_2 = 1°$.

Anisotropy in the loop frame

In the previous sections, the two fast decay components of the anisotropy decay were tentatively attributed to the local wobbling of the dye on the surface of the protein. It was assumed that the second decay component (A_2, ϕ_2, cf. Table 1) probes the motion of the loop to which the dye is attached.

This assumption is tested here by directly calculating from the simulation the ''correct'' decay component (A_{loop}, ϕ_{loop}) that is due to the loop motion. To this aim, the anisotropy decay curve $r_{\mathrm{pf}}(t)$ calculated above in the coordinate frame of

TABLE 1 Results from the fits to the experimental and simulated anisotropy decays (cf. Fig. 12) using Eq. 6 as the model function, which describes the cone-in-a-cone model

	Experiment	Simulation
A_1	0.34 ± 0.1 (46 ± 4°)	0.39 ± 0.02 (44 ± 1°)
ϕ_1	(0.41 ± 0.03) ns	(0.120 ± 0.005) ns
A_2	0.067 ± 0.02 (68 ± 1°)	0.32 ± 0.02 (47 ± 1°)
ϕ_2	(0.92 ± 0.2) ns	(0.98 ± 0.12) ns
ϕ_G	5.0 ns	3.9 ns

Values in parenthesis are the corresponding semicone angles (Eq. 4).

the protein (Figs. 12 *C* and 13, *dashed line*) is compared to the decay curve $r_{lf}(t)$ calculated in the loop frame (Fig. 13, *solid line*). The difference between these two curves is only due to the loop motion.

The motion of the dye in the protein frame can be described as the motion of the dye in the loop frame superimposed by the motion of the loop. In the framework of the cone-in-a-cone model (see Methods), the corresponding anisotropy $r_{pf}(t)$ in the protein frame is, thus, given by

$$r_{pf}(t) = r_{lf}(t)[(1 - A_{loop})e^{-t/\phi_{loop}} + A_{loop}]. \qquad (17)$$

To obtain $r_{lf}(t)$, all structures from the original MD trajectory have been fitted onto the loop residues 30–42. The inset in Fig. 13 shows several such protein snapshots superimposed. The parameters $A_{loop} = 0.77$ and $\phi_{loop} = 1370$ ps are determined from Eq. 17 by fitting. The decay time ϕ_{loop} of this component matches well to the decay time ϕ_2, but the amplitude A_{loop} is significantly larger than A_2, i.e., the corresponding semicone angle is smaller. From this we conclude, that the loop motion alone is not sufficient to account for the second decay component (A_2, ϕ_2). This indicates that there must be a further decay component in $r_{lf}(t)$ that additionally contributes to the depolarization at the timescale of ~1 ns.

Because we observed a flipping of the dye between two orientations in conformation A, as described above (cf. Fig. 8), which occurs roughly on the same timescale (three orientation flip events in 10 ns) as the slow correlation times ϕ_{loop} and ϕ_2, we suppose this process to be the missing additional component in $r_{lf}(t)$. That means, there are actually two processes, contributing to the slow (second) component in the experimental anisotropy, the flipping of the dye orientation and the loop flexibility, which both occur at the same timescale and therefore cannot be resolved by the ex-

periment alone. The straight use of the cone-in-a-cone model to interpret the measured anisotropy decay would therefore overestimate the absolute amplitude of the loop flexibility.

Orientation distribution of the dye

To test whether the wobbling-in-a-cone model is appropriate to describe the local wobbling of the dye, the orientation distribution of the transition dipole moment was calculated for both dye conformations, A and B. Fig. 14 shows these orientation distributions, calculated as described in Methods. Both distributions are unimodal and resemble Gaussian distributions. The width of the distribution in conformation A, 44°, is broader than that in conformation B, 29°. The shapes of the distributions are well approximated by Gaussian distributions. The semicone angles obtained by a wobbling-in-a-cone analysis of the simulated anisotropy, 40 and 27° for A and B, respectively, agree very well to the obtained widths of the distributions, as has already been shown (45). We conclude that the wobbling-in-a-cone model describes the fast local wobbling of the dye sufficiently accurate, if the cone angle is interpreted as the effective width of the orientational distribution of the transition dipole moments.

SUMMARY

Aiming at an atomistic interpretation of time-resolved fluorescence anisotropy experiments, we have carried out
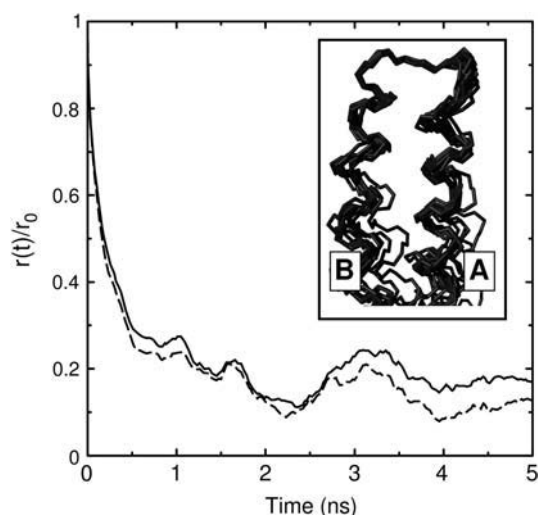

FIGURE 13 Calculated anisotropy decay of the dye in conformation A in the protein frame (*dashed line*) and in the loop frame (*solid line*). The inset shows several superimposed protein structures from the trajectory, which is fitted onto the loop residues.
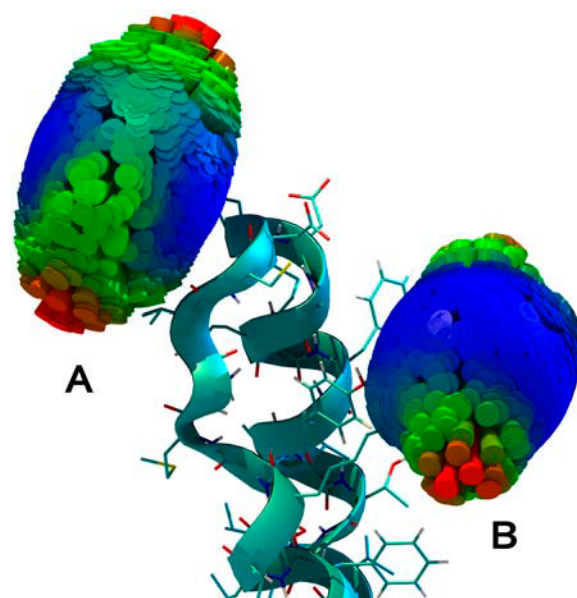

FIGURE 14 Orientation distribution of the transition dipole moment of the dye in both conformations A and B, represented by cones placed at the surface of a sphere. The color and the lengths of the cones denote the frequency that the transition dipole moment adopts a certain direction (*red*, *green*, and *blue* means high, mid-, and low frequency, respectively). The two orientation distributions are centered at the mean position of the dye in conformation A or B, respectively.

molecular dynamics simulations in close resemblance to the experimental situation. Here we have focused on the analysis of fluorescence depolarization measurements of the loop mobility of bacteriorhodopsin (bR). In these experiments, an Alexa488 dye has been attached to the loop within the AB fragment of bR. Our simulations revealed two possible conformations of the dye. It was observed that the mobility of the dye differs significantly for these two conformations. Analysis of the electrostatic interactions suggested one of the dye conformations to be the dominant one that, therefore, is mainly observed in the experiment.

By comparison with a second simulation of the protein without the dye, the influence of the dye on the dynamics of the protein was found to be small, the only significant effect being a small decrease (maximum 15%) of the loop fluctuations due to the bound dye. This finding supports the usual assumption made in the experiments that the dye does not severely affect the protein dynamics.

To study, vice versa, how the dye motion is influenced by the protein, correlations between the dye and the protein motion were analyzed in more detail, using the LMLA algorithm. This calculation revealed those residues that affect the dye motion and that are therefore mainly probed in the experiment. This information is crucial for the atomistic interpretation of the experiment and cannot be inferred from experiment alone.

Overall, the agreement between calculated and measured anisotropy is very good. The calculated anisotropy in the protein frame shows two decay components of 120 and 980 ps compared to 410 and 920 ps in the experiment. The first decay time is attributed to the rotational diffusion of the dye in the solvent (methanol); thus this fast component is due to the local wobbling of the dye. It has been described previously (43) that, generally, rotational diffusion coefficients of small compounds are quite sensitive to force-field effects, hence the discrepancy for the rotational diffusion. Our assignment is not affected by this possible artifact.

The second component of 980 ps has initially been attributed to the protein flexibility. To further test this assumption, the anisotropy was calculated in the coordinate frame of the loop, which allowed to directly assess the influence of the loop flexibility onto the anisotropy. It was found that the decay time of the depolarization induced by the loop (1370 ps) is indeed close to the second component. Further evidence for the assignment of the rotational correlation time to the loop dynamics is provided by NMR experiments, which show that the backbone N-H vectors are involved in a 1-ns dynamics (37). However, the loop motion alone can only explain part of the second component. We propose the missing additional contribution to the depolarization on the timescale of ~1 ns to be due to the transition of the dye between the two conformational substates (''up'' and ''down''), observed in our simulations. The differentiation between these two processes (the loop flexibility and the conformational transition of the dye) provided an interpretation that is not accessible to the experiment. Furthermore, because these two processes in the particular dye-loop construct that we have investigated contribute to the measured depolarization on the same timescale, straightforward application of the conventional cone-in-a-cone model to the anisotropy decay curve, would overestimate the cone angle of the protein cone, i.e., the loop flexibility.

REFERENCES

1. Weiss, S. 1999. Fluorescence spectroscopy of single biomolecules. *Science*. 283:1676–1683.

2. Schuler, B., A. Lipman, and W. A. Eaton. 2002. Probing the free energy surface for protein folding with single molecule fluorescence spectroscopy. *Nature*. 419:743–747.

3. Margittai, M., J. Widengren, E. Schweinberger, G. F. Schröder, S. Felekyan, E. Haustein, M. König, D. Fasshauer, H. Grubmüller, R. Jahn, and C. A. M. Seidel. 2003. Single-molecule fluorescence resonance energy transfer reveals a dynamic equilibrium between closed and open conformations of syntaxin 1. *Proc. Natl. Acad. Sci. USA*. 100:15516–15521.

4. McKinney, S. A., A.-C. Déclais, D. M. J. Lilley, and T. Ha. 2003. Structural dynamics if individual Holliday junctions. *Nat. Struct. Biol.* 10:93–97.

5. Schröder, G. F., and H. Grubmüller. 2003. Maximum likelihood trajectories from single molecule fluorescence resonance energy transfer. *J. Chem. Phys.* 119:9920–9924.

6. Munro, I., I. Pecht, and L. Stryer. 1979. Subnanosecond motions of tryptophan residues in proteins. *Proc. Natl. Acad. Sci. USA*. 76:56–60.

7. Juszczak, L. J., Z.-Y. Zhang, L. Wu, D. S. Gottfried, and D. D. Eads. 1997. Rapid loop dynamics of Yersinia protein tyrosine phosphatases. *Biochemistry*. 36:2227–2236.

8. Alexiev, U., I. Rimke, and T. Pöhlmann. 2003. Elucidation of the nature of the conformational changes of the EF-interhelical loop in bacteriorhodopsin and of the helix VIII on the cytoplasmic surface of bovine rhodopsin: a time-resolved fluorescence depolarization study. *J. Mol. Biol.* 328:705–719.

9. Kinosita, K., S. Kawato, and A. Ikegami. 1977. A theory of fluorescence polarization decay in membranes. *Biophys. J.* 20:289–305.

10. Szabo, A. 1984. Theory of fluorescence depolarization in macromolecules and membranes. *J. Chem. Phys.* 81:150–167.

11. Wallach, D. 1967. Effect of internal rotation on angular correlation functions. *J. Chem. Phys.* 47:5258–5268.

12. Lipari, G., and A. Szabo. 1980. Effect of librational motion on fluorescence depolarization and nuclear magnetic-resonance relaxation in macromolecules and membranes. *Biophys. J.* 30:489–506.

13. Levy, R. M., and A. Szabo. 1982. Initial fluorescence depolarization of tyrosines in proteins. *J. Am. Chem. Soc.* 104:2073–2075.

14. Ichiye, T., and M. Karplus. 1983. Fluorescence depolarization of tryptophan residues in proteins: a molecular dynamics study. *Biochemistry*. 22:2884–2893.

15. Henry, E. R., and R. Hochstrasser. 1987. Molecular dynamics simulations of fluorescence polarization of tryptophans in myoglobin. *Proc. Natl. Acad. Sci. USA*. 84:6142–6146.

16. Axelsen, P. H., C. Haydock, and F. G. Prendergast. 1988. Molecular dynamics of tryptophan in ribonuclease-T1. *Biophys. J.* 54:249–258.

17. Ringhofer, S., J. Kallen, R. Dutzler, A. Billich, A. J. W. G. Visser, D. Scholz, O. Steinhauser, H. Schreiber, M. Auer, and A. J. Kungl. 1999. X-ray structure and conformational dynamics of the HIV-1 protease in complex with the inhibitor SDZ283–910: agreement of time-resolved spectroscopy and molecular dynamics simulations. *J. Mol. Biol.* 286:1147–1159.

18. Shi, J., K. Tai, J. A. McCammon, P. Taylor, and D. A. Johnson. 2003. Nanosecond dynamics of the mouse acetylcholinesterase cys^{69}-cys^{96} omega loop. *J. Biol. Chem.* 278:30905–30911.

19. Jas, G. S., Y. Wang, S. W. Pauls, C. K. Johnson, and K. Kuczera. 1997. Influence of temperature and viscosity on anthracene rotational diffusion in organic solvents: molecular dynamics simulations and fluorescence anisotropy study. *J. Chem. Phys.* 107:8800–8812.

20. Jas, G. S., E. J. Larson, C. K. Johnson, and K. Kuczera. 2000. Microscopic details of rotational diffusion of perylene in organic solvents: molecular dynamics simulation and experiment vs Debye-Stokes-Einstein theory. *J. Phys. Chem. A.* 104:9841–9852.

21. Daura, X., R. Suter, and W. F. van Gunsteren. 1999. Validation of molecular simulation by comparison with experiment: rotational re-orientation of tryptophan in water. *J. Chem. Phys.* 110:3049–3055.

22. Mark, P., and L. Nilsson. 2002. A molecular dynamics study of tryptophan in water. *J. Phys. Chem. B.* 106:9440–9445.

23. Sakmar, T. P., S. T. Menon, E. P. Marin, and E. S. Awad. 2002. Rhodopsin: insights from recent structural studies. *Annu. Rev. Biophys. Biomol. Struct.* 31:443–484.

24. Marshall, G. R. 2001. Peptide interactions with G-protein coupled receptors. *Biopolymers.* 60:246–277.

25. Tao, T. 1969. Time-dependent fluorescence depolarization and Brownian rotational diffusion coefficients of macromolecules. *Biopolymers.* 8:609–632.

26. Alexiev, U., R. Mollaaghababa, P. Scherrer, H. G. Khorana, and M. P. Heyn. 1995. Rapid long-range proton diffusion along the surface of the purple membrane and delayed proton transfer into the bulk. *Proc. Natl. Acad. Sci. USA.* 92:372–376.

27. Liao, M.-J., E. London, and H. G. Khorana. 1983. Regeneration of native bacteriorhodopsin structure from two chymotryptic fragments. *J. Biol. Chem.* 258:9949–9955.

28. Scherrer, P., U. Alexiev, T. Marti, H. G. Khorana, and M. P. Heyn. 1994. Covalently bound pH-indicator dyes at selected extracellular or cytoplasmic sites in bacteriorhodopsin. I. Proton migration along the surface of bacteriorhodopsin micelles and its delayed transfer from surface to bulk. *Biochemistry.* 33:13684–13692.

29. Alexiev, U., T. Marti, M. P. Heyn, H. G. Khorana, and P. Scherrer. 1994. Surface charge of bacteriorhodopsin detected with covalently bound pH-indicators at selected extracellular and cytoplasmic sites. *Biochemistry.* 33:298–306.

30. Popot, J.-L., S.-E. Gerchman, and D. M. Engelman. 1987. Refolding of bacteriorhodopsin in lipid bilayers. A thermodynamically controlled two-state process. *J. Mol. Biol.* 198:655–676.

31. Berendsen, H. J. C., D. van der Spoel, and R. van Drunen. 1995. GROMACS: a message-passing parallel molecular dynamics implementation. *Comput. Phys. Commun.* 91:43–56.

32. Berendsen, H. J. C., J. P. M. Postma, W. F. V. Gunsteren, and J. Hermans. 1981. Intermolecular Forces. B. Pullman, editor. Reidel, Dordrecht, The Netherlands.

33. Berendsen, H. J. C., J. P. M. Postma, W. F. V. Gunsteren, A. DiNola, and J. R. Haak. 1984. Molecular dynamics with a coupling to an external bath. *J. Chem. Phys.* 81:3684–3690.

34. Hess, B., H. Bekker, H. J. C. Berendsen, and J. G. E. M. Fraaije. 1997. A linear constraint solver for molecular simulations. *J. Comput. Chem.* 18:1463–1472.

35. Darden, T., D. York, and L. Pedersen. 1993. Particle mesh Ewald: an N log N method for Ewald sums in large systems. *J. Chem. Phys.* 98:10089–10092.

36. Pebay-Peyroula, E., G. Rummel, J. P. Rosenbusch, and E. M. Landau. 1997. X-ray structure of bacteriorhodopsin at 2.5 Angstroms from microcrystals grown in lipidic cubic phases. *Science.* 277:1676–1681.

37. Orekhov, V. Y., K. V. Pervushin, and A. S. Arseniev. 1994. Backbone dynamics of (1–71)bacteriorhodopsin studied by two-dimensional ^{1}H-^{15}N NMR spectroscopy. *Eur. J. Biochem.* 219:887–896.

38. Accelrys. 1996. DMol Version 960, Density Functional Theory Electronic Structure Program. Molecular Simulations, Inc., San Diego, CA.

39. Frisch, M. J., G. W. Trucks, H. B. Schlegel, G. E. Scuseria, M. A. Robb, J. R. Cheeseman, V. G. Zakrzewski, J. A. Montgomery Jr., R. E. Stratmann, J. C. Burant, S. Dapprich, J. M. Millam, and others. 1998. Gaussian 98, Revision A.5. Gaussian, Inc., Pittsburgh PA.

40. Stewart, J. P. 1989. MOPAC 5.0. Stewart Computational Chemistry, Colorado Springs, CO.

41. Singh, U. C., and P. A. Kollman. 1984. An approach to computing electrostatic charges for molecules. *J. Comput. Chem.* 5:129–145.

42. Bucher, M., and T. L. Porter. 1986. Analysis of the Born model for hydration of ions. *J. Phys. Chem.* 90:3406–3411.

43. Schröder, G. F. 2004. Simulation of Fluorescence Spectroscopy Experiments. PhD thesis. Universität Göttingen, Göttingen, Germany.

44. Lee, S., and M. Karplus. 1984. Brownian dynamics simulations: statistical error of correlation-functions. *J. Chem. Phys.* 81:6106–6118.

45. Kinosita, K., A. Ikegami, and S. Kawato. 1982. On the wobbling-in-a-cone analysis of fluorescence anisotropy decay. *Biophys. J.* 37:461–464.